Journal of Ocean, Mechanical and Aerospace
-Science and Engineering-, Vol.49

November 30, 2017

CFD Analysis of Unsteady Yaw Motion of A Towed Ship

A. Fitriadhy [a,*], N. Aqilah Mansor [b] and N. Adlina Aldin [b]

[a)] *Programme of Maritime Technology, School of Ocean Engineering, Universiti Malaysia Terengganu, Malaysia*
[b)] *Postgraduate Students Programme of Maritime Technology, School of Ocean Engineering, Universiti Malaysia Terengganu, Malaysia*

*Corresponding author: a.fitriadhy@umt.edu.my

Paper History

Received: 10-October-2017
Received in revised form: 6-November-2017
Accepted: 30-November-2017

ABSTRACT

Instability of a towed ship presented in the form of her unstable yaw motion may lead to serious accident especially at the restricted waterways such as colliding with other ships or onshore structures. To stabilize this unsteady yaw motion, a comprehensive investigation is then required to ensure a safety of ship's towing navigation. This paper presents a computational fluid dynamic (CFD) approach to analyse yaw motion characteristics of a towed ship incorporated with an asymmetrical bridle towline model. Several towing parameters such as towing's angles and speeds have taken into account. Here, a towed ship or barge in then called as 1B is employed in this simulation. The results revealed that the subsequent increase of towing's angle dealt with a better yaw motion of 1B indicated by sufficient reduction of her sway motion associated with more steady yaw motion of a towed ship.

KEY WORDS: *CFD, yaw motion, towing's angle, towing's speed and sway motion*

1.0 INTRDUCTION

Safe navigation of ship's towing system at sea is very important especially in congested areas to avoid accidents. However, in presence of the towing's instability due to large amplitude of the yaw motion hasled to a serious towing's accident such as colliding with other ships or onshore structures. To ensure a safety ship's towing navigation; therefore, a comprehensive investigation is obviously required.

Several researchers have investigated on course stability of the ship towing performances incorporated with single and symmetrical towline models. Through employing the symmetrical bridle towline, Fitriadhy and Yasukawa (2011) studied the effects towline lengths and towing points on the bridle towline model for the unstable towed ship (2B). The results showed that the course stability of 2B had been gradually improved through significant attenuation of the sway motion. In addition, Fitriadhy et al. (2013) analyzed the course stability of towed ship in single towline model in wind. The results revealed that the unstable towed ship was recovered in the range of beam to quartering winds but the towing stability of the stable towed ship in head and following winds gradually degraded. Bernitsas and Kekridis (1985) simulate the surge, sway and yaw motions and study the stability of a towed vessel by a non-linear elastic rope. Bernitsas and Chung (1990) study the stability of the symmetrical towed ship towed by two tug boats with different types of cables used as towing lines. Referring to the single and the bridle symmetrical towline models, the course stability of the towed ship has been still need to be improved. A more appropriate analysis on course stability of the towed ship using another towline model configuration, which deals with a better course stability is therefore required.

This paper proposes an analysis on course stability of a towed ship using an asymmetrical bridle towline model by using Computational Fluid Dynamic (CFD). The CFD software give more advantages compared to numerical and analytical method as it can capture the non-linear phenomenon during the computation. Besides, it also reduces the computation time and provides more accurate results for this study on course stability of ship towing system. Tow angle and speed of the barge is taken into account during the simulation to investigate the stability of the barge.

2.0 GOVERNING EQUATION

FLOW-3D solves Navier-stokes type equations embedded with various turbulence models. In this paper, RANS equations are solved with standard k-e turbulence model and Volume of Fluid (VOF) method is applied to track the free surface elevation. The interface between fluid and solid boundaries is simulated with the fractional area volume obstacle representation favour method. This method computes open area and volume in each cell to define the area that is occupied by obstacle. Mathematically, fluid flow and rigid body motion is described by conservation equations for mass and momentum. The equations for mass and momentum result in a system of four coupled nonlinear partial differential equations known as the Navier-Stokes equations.

The continuity and momentum equations for a moving object and the relative transport equation for the volume of fluid (VOF) function are

$$\frac{V_f}{\rho}\frac{\partial \rho}{\partial t}+\frac{1}{\rho}\nabla\cdot\left(\rho\vec{u}A_f\right)=-\frac{\partial V_f}{\partial t} \quad (1)$$

(Spalart and Allmaras)

$$\frac{\partial \vec{u}}{\partial t}+\frac{1}{V_f}\left(\vec{u}A_f\cdot\nabla\vec{u}\right)=-\frac{1}{\rho}\left[\nabla_p+\nabla\cdot\left(\tau A_f\right)\right]+\vec{G} \quad (2)$$

$$\frac{\partial F}{\partial t}+\frac{1}{V_f}\nabla.\left(F\vec{u}A_f\right)=-\frac{F}{V_f}\frac{\partial V_f}{\partial t} \quad (3)$$

where ρ is the density of the fluid, $\vec{u}$ fluid velocity, V_f volume fraction, A_f area fraction, P pressure, τ viscous stress tensor, G gravity and F fluid fraction.

In the case of coupled GMO's motion, equations (Spalart and Allmaras) and (2) are solved at each time step and the location of all moving objects is recorded and the area and volume fractions updated using then FAVOR technique. Equations (5) and (7) are solved with the source term $\left(-\frac{\partial V_f}{\partial t}\right)$ on the right-hand side which is computed as

$$-\frac{\partial V_f}{\partial t}=\vec{U}_{obj}.\vec{n}S_{obj}/V_{cell} \quad (4)$$

where $S_{obj}$is the surface area, $\vec{n}$ surface normal vector, $\vec{u}_{obj}$is the velocity of the moving object at a mesh cell and V_{cell} is the total volume of the cell. (*FLOW-3D 10.1.1 User Manual*, 2013).

Note that $k-\varepsilon$ model is quite economical in terms of CPU time, compared to, for example the SST turbulence model, which increases the required CPU times by nearly 25%. $k-\varepsilon$ turbulence model has also been used in many studies performed in the same area such as (Tezdogan et al., 2016) and (Wu et al., 2011). (Talaat et al., 2017) states $k-\varepsilon$ model reduced the computational time and resources by reducing the number of nodes in the near wall regions, which allow for more probing simulations and trial geometries.

The transport equation for k_T includes the convection and diffusion of the turbulent kinetic energy, the production of turbulent kinetic energy due to shearing and buoyancy effects, diffusion, and dissipation due to viscous losses within the turbulent eddies. Buoyancy production only occurs if there is a non-uniform density in the flow, and includes the effects of gravity and non-inertial accelerations. The transport equation is:

$$\frac{\partial k_T}{\partial t}+\frac{1}{V_F}\left\{uA_x\frac{\partial k_T}{\partial x}+vA_y\frac{\partial k_T}{\partial y}+wA_z\frac{\partial k_T}{\partial z}\right\}=P_T+G_T+Diff_{k_T}-\varepsilon_T \quad (5)$$

where $V_F, A_x, A_y and A_z$ are FLOW-3D's FAVOR™ functions, P_T is the turbulent kinetic energy production:

$$P_T=CSPRO\left(\frac{\mu}{pV_F}\right)\times\left\{\begin{matrix}2A_x\left(\frac{\partial\mu}{\partial x}\right)^2+2A_y\left(R\frac{\partial v}{\partial y}\xi\frac{u}{x}\right)^2+2A_z\left(\frac{\partial w}{\partial z}\right)^2\\+\left(\frac{\partial v}{\partial x}+R\frac{\partial \mu}{\partial y}+\xi\frac{v}{x}\right)\left[A_x\frac{\partial v}{\partial x}+A_y\left(R\frac{\partial u}{\partial y}+\xi\frac{v}{x}\right)\right]\\+\left(\frac{\partial u}{\partial z}+\frac{\partial w}{\partial x}\right)\left(A_z\frac{\partial u}{\partial z}+A_x\left(R\frac{\partial w}{\partial x}\right)\right)\\+\left(\frac{\partial v}{\partial z}+R\frac{\partial w}{\partial y}\right)\left(A_z\frac{\partial v}{\partial z}+A_yR\frac{\partial w}{\partial y}\right)\end{matrix}\right\} \quad (6)$$

where CSPRO is a turbulence parameter.

In the case of this computation for turbulent condition, $k-\varepsilon$ model is proposed where k_T is turbulent kinetic energy and ε_T is turbulent dissipation energy. A more sophisticated – and more widely used – model consists of two transport equations for the turbulent kinetic energy k_T and its dissipation ε_T, the so-called$k-\varepsilon$ model (Harlow-Nakayama, 1967). The $k-\varepsilon$ model has been shown to provide reasonable approximations to many types of flows (Rodi, 1980).

The body motion is analyzed in a space-fixed Cartesian coordinate system, the global coordinate system. The governing equation of the six degree of freedom (DOF) of a rigid body motion can be expressed in this coordinate system as

$$\frac{d}{dt}(m\vec{v}_C)=\vec{f} \quad (7)$$

$$\frac{d}{dt}(M_C.\vec{\omega}_C)=\vec{m}_C \quad (8)$$

The index C denotes the center of mass of the body, m denotes the mass of the body, $\vec{v}_C$ the velocity vector, M_C the tensor of the moments of inertia, $\vec{\omega}_c$ the angular velocity vector, $\vec{f}$ the resulting force vector and $\vec{m}_c$the resultant moment vector acting on the body (Wu et al., 2011).

The resultant forces f has three components; surface force, field forces and external forces:

$$\vec{f}=\int_S(T-\rho I).\vec{n}dS+\int_V\rho_b\vec{b}dV+\vec{f}E \quad (9)$$

ρ_b is the density of the body. The only field force considered is gravity, so the volume integral of above equation (right hand side) reduces to $m\vec{g}$, where $\vec{g}$ is the gravity acceleration vector. The vector $\vec{f}E$ denotes the external forces acting in the body. (Yan and Huang, 1996)

JOMAse | Received: 10-October-2017 | Accepted: 30-November-2017 | [(49) 1: 1-13]
Published by International Society of Ocean, Mechanical and Aerospace Scientists and Engineers, www.isomase.org., ISSN: 2354-7065 & e-ISSN: 2527-6085

3.0 SIMULATION CONDITION

3.1 Principle Data of Ship

The dimension of the barge is presented in Table 1 while the barge model used in the CFD simulation is shown in Figure 1.

Table 1: Barge dimension

Description	Dimension
Length *l*,(m)	1.221
Breadth *b*, (m)	0.213
Draft *d*, (m)	0.0548
Volume *V*,(m^3)	0.02634
L/B	2.86
Block coefficient C_b	0.92

a) Barge model

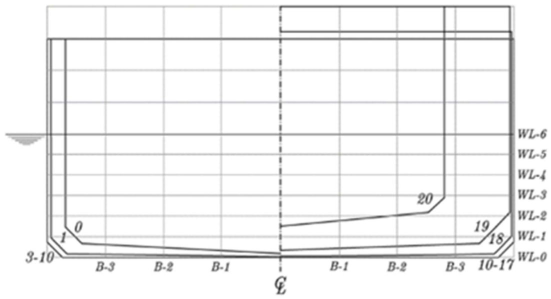

b) Barge body plan

Figure 1: Barge model and body plan used in CFD simulation

3.2 Simulation Parameter

Figure 2 shows the towing condition of the towed barge. The tug is replaced with the sphere by using similar characteristics of tug. This is to reduce the computational time during simulation. The simulation parameters used in this analysis are shown in Table 2. The tow angle used varies from 10 to 40 degree at constant speed while variation of speeds are used at constant tow angle 30 degree. The actual speed of 7 knot to 10 knot is equivalent to model speed 0.509 m/s to 0.728 m/s and as shown in the table 2.

Table 2: Barge towing parameter

Tow angle, α (°)	Speed (m/s)
10°	0.509
20°	
30°	
40°	

Tow angle, α (°)	Speed (m/s)
30°	0.509
	0.582
	0.655
	0.728

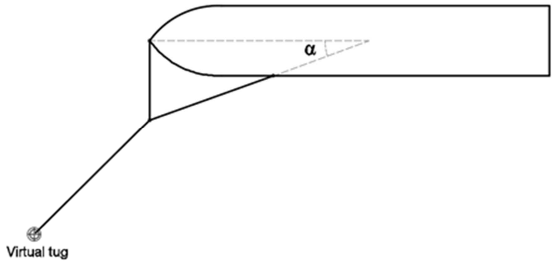

Figure 2: Simulation condition of barge

3.3 Computational Domain and Meshing Generation

The computational domain of the barge associated with the number of meshing cell in the CFD. The total number of cells used in the simulation is 1,300,000.

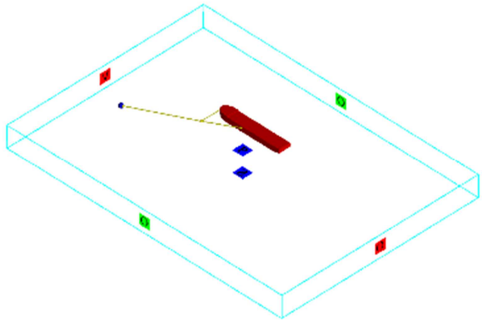

(a) Boundary condition

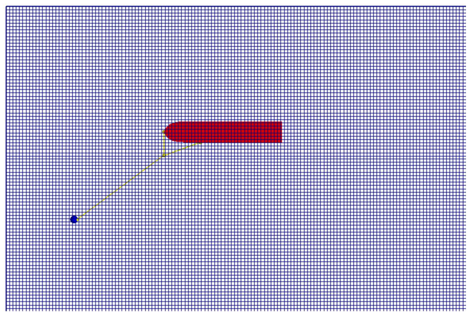

(b) Meshing generation

Figure 3: Meshing boundary condition of barge

Referring to Figure 3, the boundary conditions are mark in the mesh block. The boundary condition at X-max boundary is specified velocity so that there is flow of water in the boundary. The velocity used in the simulation varies from 0.509 m/s to 0.728 m/s for the sphere model. For X-min, Y-max and Y-min use outflow boundary to absorb the wave motion which will reduce the reflection from the boundary while Z-min using symmetry boundary which it applies zero-gradient condition at the boundary and Z-max using specified pressure to create a uniform pressure in the boundary. The boundary conditions for this simulation are as shown in Table 3.

JOMAse | Received: 10-October-2017 | Accepted: 30-November-2017 | [(49) 1: 1-13]
Published by International Society of Ocean, Mechanical and Aerospace Scientists and Engineers, www.isomase.org., ISSN: 2354-7065 & e-ISSN: 2527-6085

Table 3: Boundary Conditions

Boundary	Mesh block
X_{min}	Specified Velocity
X_{max}	Outflow
Y_{min}	Outflow
Y_{max}	Outflow
Z_{min}	Symmetry
Z_{max}	Specified pressure

The barge is coupled through a towline. Sphere model which acted as the tow ship is assigned as prescribed motion while barge as towed ship is set as coupled motion in X translational, Y translational and Z rotational motions (surge, sway and yaw as this simulation is considering 3 degree of freedom. The towline is set as massless elastic rope with spring coefficient of 1297.6 kg/s^2 and 648.8 kg/s^2.

Based on the applications of FLOW3D v11.0.4, the average duration of every simulation was about 70-80 hours (4 parallel computations) on a HP Z820 workstation PC with processor Intel (R) Xeon (R) CPU ES-2690 v2 @ 3.00 GHz (2 processors) associated with the installed memory of 32.0 GB and 64-bit Operating System.

4.0 RESULT AND DISCUSSION

4.1 Effect of tow angle of unsteady yaw motion of barge

By using CFD simulation approach, the analysis of course stability of towed ship is successfully conducted. The simulation results are presented, along with the discussion of the analysis of the towline model of towed ship.

Figure 5 concludes the sway motion of the barge for different tow angle from 10 to 40 degree. Regardless of various tow angles, the results showed the subsequent decreases of sway motion of the asymmetrical barge. The tow angle at 10 degree shows uniform sway motion and it decreasing when reaching 30 and 40 degree. Tow angle at 40 degree shows the most stable towing as it shows almost zero sway motion at 30 s compared to 30 degree at 40 s.

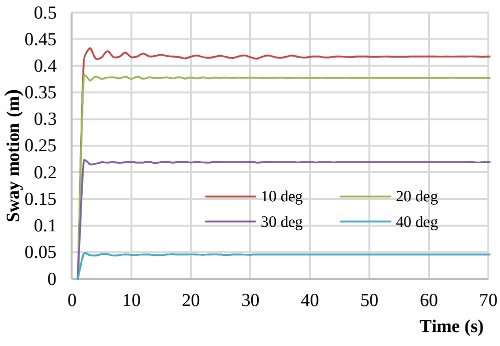

Figure 5: The effect of sway motion of asymmetrical towing in various tow angle

Figure 6 shows that the yaw motion of the asymmetrical towing in different tow angles from 10 degree to 40 degree. At the initial moment of simulation, there are increase of yaw motion of barge at all angles and they slowly decrease as the time increase.

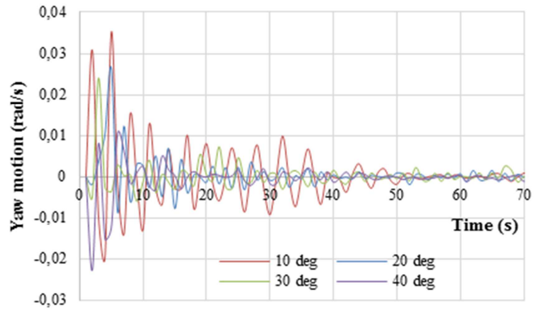

Figure 6: The effect of yaw motion of asymmetrical towing in various tow angle

The effect of yaw motion decreasing from 10 to 40 degree which the 10 degree has the highest yaw motion compared to others while 40 degree shows that the yaw motion has decreased early compared to 30 degree of tow angle. From the results, it can be validated with the research by Zan et.al, (2012) who did the experimental research which shows nearly zero sway motion of asymmetrical towing compared to symmetrical towed ship. Fitriadhy et al. (2014) investigated on the bridle towline model to stabilize ship towing performance by using numerical method with focusing on tow angle and tow point. The results of the research revealed that the asymmetrical towed ship is better compared to symmetrical towed ship in term of course stability that reduce the sway and yaw motion of barge.

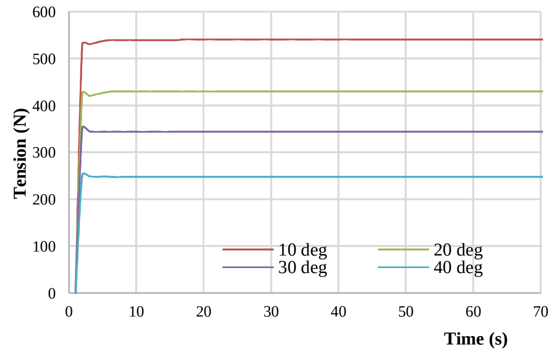

Figure 7: The effect of towline tension of asymmetrical towing in various tow angle

Figure 7 shows the effect of towline tension of the asymmetrical towing in various tow angle. Tow angle at 10 degree has the highest towline tension compared to tow angle at 40 deg which has the lowest towline tension. It can be conclude that the lowest angle has the highest towline tension. This possibly occur due to high acceleration of barge surge motion. Figure 8 shows the visualization of asymmetrical towing simulation in various tow angle at 10 to 40 degree. Figure 8 below shows the CFD visualization of asymmetrical towing simulation in various tow angle. Figure shows the visualization of asymmetrical towing simulation in various tow angle from 10 to 40 degree. As shown in Figure 8, the further increase of angle resulted in having less effect of wave crest on the fluid around the barge with higher wave crest at 10 degree.

JOMAse | Received: 10-October-2017 | Accepted: 30-November-2017 | [(49) 1: 1-13]
Published by International Society of Ocean, Mechanical and Aerospace Scientists and Engineers, www.isomase.org., ISSN: 2354-7065 & e-ISSN: 2527-6085

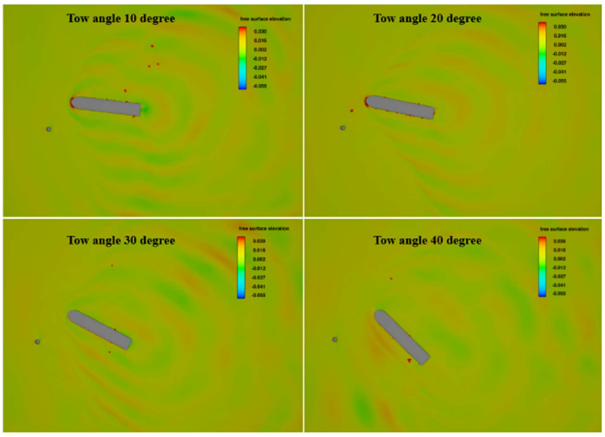

Figure 8: CFD visualization of asymmetrical towing simulation in various tow angle, α

4.2 Effect of tow speed of unsteady yaw motion of barge

Figure 9 concludes the sway motion of the barge for various tow speed from 0.509 m/s to 0.728 m/s at tow angle 30 degree. Regardless of various tow speed, the results showed the subsequent decreases of sway motion of the asymmetrical barge at 0.509 m/s. The tow speed at 0.509 m/s shows decrease of sway motion compared to 0.582 m/s, 0.655 m/s and 0.728 m/s. All the towing speeds show their almost stable sway motion at 50 s.

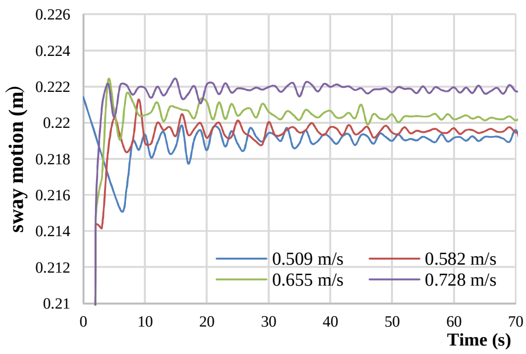

Figure 9: The effect of sway motion of asymmetrical towing in various tow speed

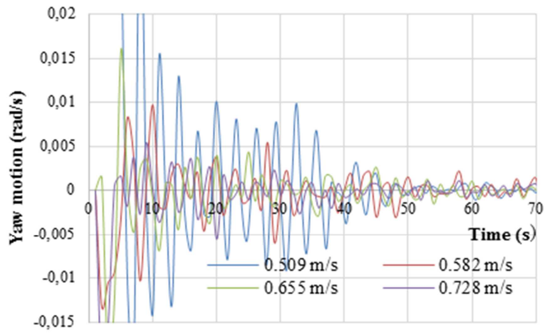

Figure 10: The effect of yaw motion of asymmetrical towing in various tow speed

Figure 10 shows that the yaw motion of the asymmetrical towing in different tow speed from 0.509 m/s to 0.728 m/s. At the initial moment of simulation, there are increase of yaw motion at all angles and they slowly decrease as the time increase. The effect of yaw motion decreasing from 0.509 m/s to 0.728 m/s of speed which the 0.509 m/s has the highest yaw motion compared to others while 0.728 m/s shows that the yaw motion has decreased.

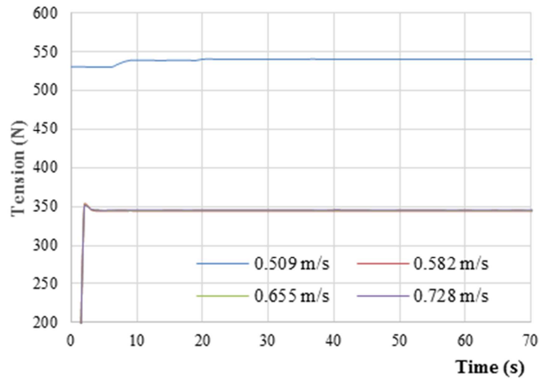

Figure 11: The effect of towline tension of asymmetrical towing in various tow speed

Figure 11 shows the graph on the effect of towline tension of asymmetrical ship towing in various tow speed. The results show that tow speed at 0.509 m/s has the highest towline tension compared to 0.582 m/s, 0.655 m/s and 0.728 m/s which show the same towline tension. Figure 12 shows the visualization of asymmetrical towing simulation in various tow speed from 0.509 m/s to 0.728 m/s. As shown in Figure 12, the further increase of speed resulted in having less effect of wave crest on the fluid around the barge.

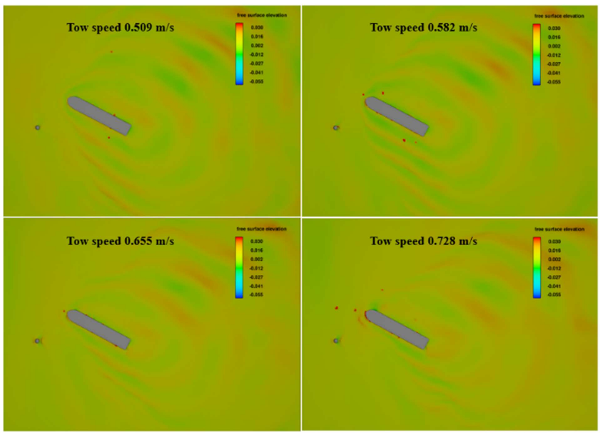

Figure 12: CFD visualization of asymmetrical towing simulation in various tow speed

JOMAse | Received: 10-October-2017 | Accepted: 30-November-2017 | [(49) 1: 1-13]
Published by International Society of Ocean, Mechanical and Aerospace Scientists and Engineers, www.isomase.org., ISSN: 2354-7065 & e-ISSN: 2527-6085

5.0 CONCLUSION

The CFD investigation on the unsteady yaw motion was successfully performed. The effect of yaw motion were examined accordingly at a wide range of tow angles and tow speeds. The computation results are drawn as follows:

- Asymmetrical towing configuration with increasing tow angle improve the course stability of towing performance.
- Sway and yaw motion at 40 degree tow angle improve the effectiveness in towing stability and safe for towing performance at sea.
- Increasing of towing speed shows higher sway motion but decreasing of its yaw motion where the speed of 0.728 m/s has better course stability.

ACKNOWLEDGEMENTS

The authors greatly appreciate to Ministry of Higher Education of Malaysia for the financial support awarded from Fundamental Research Grant Scheme (FRGS) Vot No. 59414.

REFERENCE

1. Bernitsas, M., & Kekridis, N. (1985). Simulation and stability of ship towing. *International Shipbuilding Progress, 32*(369), 112-123.
2. Bernitsas, M. M., & Chung, J.-S. (1990). Nonlinear stability and simulation of two-line ship towing and mooring. *Applied Ocean Research, 12*(2), 77-92.
3. Fitriadhy, A., & Yasukawa, H. (2011). Course Stability of a Ship Towing System. *Ship Technology Research, 58*(1), 4-23.
4. Fitriadhy, A., Yasukawa, H., & Koh, K. (2013). Course Stability of a Ship Towing System in Wind. *Ocean Engineering, 64*, 135-145.
5. Fitriadhy, A., Yasukawa, H., Yoneda, T., Kohd, K., & Maimund, A. (2014). Analysis of an Asymmetrical Bridle Towline Model to Stabilise Towing Performance of a Towed Ship. *Jurnal Teknologi (Sciences & Engineering), 66*(2), 151-156.
6. *FLOW-3D 10.1.1 User Manual*. (2013). Flow Science Inc.
7. Spalart, P., & Allmaras, S. (1992). *A one-equation turbulence model for aerodynamic flows.* Paper presented at the 30th aerospace sciences meeting and exhibit.
8. Talaat, W. M., Hafez, K., & Banawan, A. (2017). A CFD Presentation and Visualization For a New Model that Uses Interceptors to Harness Hydro-energy at the Wash of Fast Boats. *Ocean Engineering, 130*, 542-556.
9. Tezdogan, T., Incecik, A., & Turan, O. (2016). A Numerical Investigation of the Squat and Resistance of Ships Advancing through a Canal using CFD. *Journal of Marine Science and Technology, 21*(1), 86-101.
10. Wu, C.-S., Zhou, D.-C., Gao, L., & Miao, Q.-M. (2011). CFD Computation of Ship Motions and Added Resistance for a High Speed Trimaran in Regular Head Waves. *International Journal of Naval Architecture and Ocean Engineering, 3*(1), 105-110.
11. Yan, S., & Huang, G. (1996). *Dynamic Performance of Towing System-Simulation and Model Experiment.* Paper presented at the Proceedings, OCEAN.

JOMAse | Received: 10-October-2017 | Accepted: 30-November-2017 | [(49) 1: 1-13]
Published by International Society of Ocean, Mechanical and Aerospace Scientists and Engineers, www.isomase.org., ISSN: 2354-7065 & e-ISSN: 2527-6085